NANO LETTERS
Letter
Cite This: Nano Lett. 2019, 19, 4470−4477
pubs.acs.org/NanoLett

Recognition, Intervention, and Monitoring of Neutrophils in Acute Ischemic Stroke

Chunming Tang, Cong Wang, Ying Zhang, Lingjing Xue, Yanyi Li, Caoyun Ju,* and Can Zhang*

State Key Laboratory of Natural Medicines and Jiangsu Key Laboratory of Drug Discovery for Metabolic Diseases, Center of Advanced Pharmaceuticals and Biomaterials, China Pharmaceutical University, Nanjing 210009, P. R. China

Supporting Information

ABSTRACT: Neutrophils are implicated in numerous inflammatory diseases, and especially in acute ischemic stroke (AIS). The unchecked migration of neutrophils into cerebral ischemic regions, and their subsequent release of reactive oxygen species, are considered the primary causes of reperfusion injury following AIS. Reducing the infiltration of inflammatory neutrophils may therefore be a useful therapy for AIS. Here, inspired by the specific cell−cell recognition that occurs between platelets and inflammatory neutrophils, we describe platelet-mimetic nanoparticles (PTNPs) that can be used to directly recognize, intervene, and monitor inflammatory neutrophils in the AIS treatment and therapeutic evaluation. We demonstrate that PTNPs, coloaded with piceatannol, a selective spleen tyrosine kinase inhibitor, and superparamagnetic iron oxide (SPIO), a T2 contrast agent, can successfully recognize adherent neutrophils via platelet membrane coating. The loaded piceatannol could then be delivered to adherent neutrophils and detach them into circulation, thus decreasing neutrophil infiltration and reducing infarct size. Moreover, when coupled with magnetic resonance imaging, internalized SPIO could be used to monitor the inflammatory neutrophils, associated with therapeutic effects, in real time. This approach is an innovative method for both the treatment and therapeutic evaluation of AIS, and provides new insights into how to treat and monitor neutrophil-associated diseases.

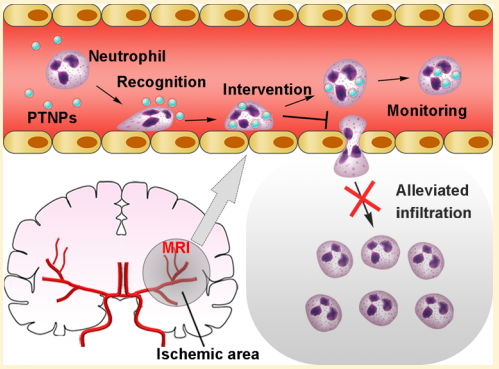

KEYWORDS: *Inflammatory neutrophil recognition, platelet-mimetic nanoparticles, piceatannol, superparamagnetic iron oxide, acute ischemic stroke*

Ischemic stroke is the leading cause of death and serious long-term disability worldwide. Early administration of recombinant tissue plasminogen activator (rtPA) is currently the only effective thrombolytic therapy for acute ischemic stroke (AIS) that is approved by the FDA.[1−3] However, rtPA treatment has a narrow therapeutic window and must be provided within 4.5 h after stroke onset. As a result, less than 5% of all patients can receive this therapy.[4−7] Moreover, therapeutic outcomes are further compromised by the secondary injuries produced by cerebral ischemia and reperfusion, which include excitotoxicity, mitochondrial response, calcium influx, free radical damage, and inflammation.[8−10] Among these processes, growing evidence has pointed to neutrophils (NEs) as a key contributor to the pathophysiology of AIS. NEs are generally the first and most abundant inflammatory cells to appear in microvascular response to ischemic stroke, especially compared with monocytes/macrophages, which migrate to cerebral ischemic regions during the whole acute phase of inflammation.[11−13] The abundant infiltrating NEs are associated with elevated reactive oxygen species (ROS) and inflammatory mediators, which worsen ischemic tissue damage.[14−17] An intervention against the infiltration of NEs into cerebral ischemic regions may therefore be an effective therapy for AIS.[18,19]

Studies have shown that stopping NEs from adhering to endothelial cells can alleviate NEs infiltration as well as prevent inflammation.[18,20−22] For example, inhibiting β2 integrin using anti-β2 integrin antibodies can effectively block the adherence of NEs to endothelial cells, but the innate bactericidal function of NEs is also reduced due to the action of antibodies.[23−25] Piceatannol, a selective spleen tyrosine kinase (Syk) inhibitor that blocks outside-in β2 integrin signaling in NEs, has been demonstrated to have a potential therapeutic effect on acute lung injury because of its prevention of neutrophil adhesion.[26] However, selective delivery of piceatannol to inflammatory NEs remains difficult. Biodegradable nanoparticles are promising carrier systems for the delivery of therapeutics to target cells through the modification of ligands or antibodies on their surfaces.[27,28] In previous studies, a small number of nanotechnologies have been developed to target NEs, including albumin nanoparticles (NPs),[26] *N*-acetyl Pro-Gly-Pro (Ac-PGP) modified liposomes,[29] and anti-CD11b-linked[30] and anti-CD177-binding[31] NPs. However, these exogenous biofunctionalized NPs cannot imitate the complex intercellular

Received: March 28, 2019
Revised: June 5, 2019
Published: June 19, 2019

DOI: 10.1021/acs.nanolett.9b01282
Nano Lett. 2019, 19, 4470−4477

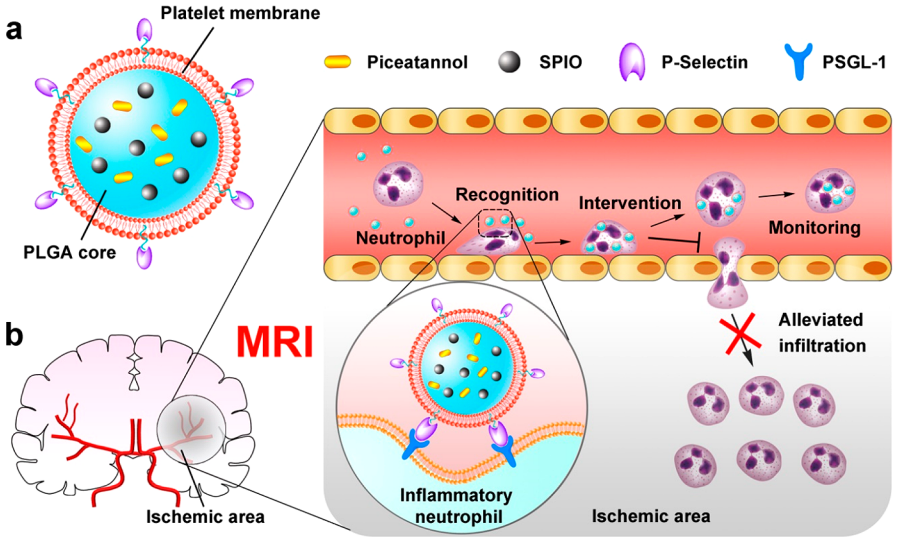

Figure 1. Effective recognition, intervention, and monitoring of inflammatory neutrophils by platelet-mimetic nanoparticles (PTNPs) for the treatment of AIS and the evaluation of their therapeutic effect. (a) A diagram of the main components of PTNPs, including the SPIO and piceatannol coloaded PLGA core and the platelet membrane coating shell. (b) After intravenous injection, PTNPs could selectively recognize inflammatory neutrophils via the specific affinity between P-selectin and the PSGL-1-bearing microdomain. PTNPs were then internalized into adherent neutrophils where the loaded piceatannol was released, thus promoting the detachment of neutrophils from endothelial cells into circulation, resulting in decreased neutrophil infiltration. When coupled with MRI, inflammatory neutrophils could be precisely monitored in real time because of the T_2 contrast agent SPIO, which indicated the therapeutic effect of PTNPs.

interactions that are present in the human body, leading to unsatisfactory specificity and biodistribution, and a relatively short circulation time.

It is well-documented that platelets act as accomplices in NEs infiltration at inflammation sites.[32,33] NEs adhering to inflamed vessels extend a P-selectin glycoprotein ligand-1 (PSGL-1)-bearing microdomain into the vessel lumen that scans for activated platelets present in the bloodstream via P-selectin. Once activated, platelets bind to the NEs and aid NEs leakage from the vessel lumen into the inflammation site.[34] These results support the idea that platelets can actively recognize adherent NEs through cell−cell recognition. In addition, the amount of infiltrated NEs in the ischemic area is closely related with the acute ischemic stroke progress.[14] Thus, a way to monitor the extent of infiltrating NEs may provide a way to evaluate therapeutic efficiency in acute ischemic stroke and further guide personalized medication.

Inspired by this idea, we designed platelet-mimetic nanoparticles (PTNPs) to discern, intervene, and monitor activated NEs in inflamed endothelial cells, which will provide a strategy for the treatment and real-time monitoring of NE-related inflammatory diseases (Figure 1). The inner core of PTNPs is composed of poly(lactic-*co*-glycolic acid) (PLGA) nanoparticles coloaded with piceatannol, for the prevention of NEs infiltration, and superparamagnetic iron oxide (SPIO), for magnetic resonance imaging (MRI), which is one of the most used noninvasive, versatile imaging modalities.[35,36] The biomimetic outer shell of PTNPs is derived from the membranes of platelets and uses the native biocompatibility and targeting efficiency of living platelets rather than their promotion of NEs infiltration.[37,38] In this way, the PTNPs exhibit immune evasion and inflammatory NEs recognition. Furthermore, we used a rodent model of transient middle cerebral artery occlusion (tMCAO) to assess the treatment and diagnosis efficacy of PTNPs. The PTNPs were expected to selectively discern the activated NEs utilizing the specific affinity between P-Selectin, on platelets, and PSGL-1, on activated NEs. After endocytosis by NEs, the incorporated piceatannol markedly reduced NEs adhesion and migration across the ischemic endothelium, thus decreasing infarct size and improving neurological outcomes in AIS. Furthermore, when coupled with MRI, the therapeutic efficacy of NEs intervention treatment could be precisely monitored in real time using the T_2 signal of SPIO within inflammatory NEs. Our study provides a novel prospect for the personalized therapy and diagnosis of AIS, which may conquer the possible risk of microbleeds or hemorrhage induced by the thrombolytic agents.

The PTNPs were composed of piceatannol and SPIO coloaded PLGA nanoparticles as the inner core and platelet membrane as the coating shell. To prepare the PTNPs, we first synthesized the oleylamine-modified SPIO using a one-pot high-temperature reductive decomposition method, as described in previous reports.[39] The crystal information and surface chemistry of SPIO were confirmed using X-ray diffractometry (XRD) and Fourier-transform infrared spectrometry (FTIR) (Figure S1), respectively. The synthesized SPIO had a narrow size distribution, with an average particle size of 10 nm, and an excellent superparamagnetism, with a magnetization saturation of 89.4 emu g^{-1} (Figure 2a; Figure S2). Next, PLGA nanoparticles (TNPs) containing piceatannol and SPIO were prepared using a simple emulsion solvent evaporation method.[40] Platelets were then collected using gradient centrifugation and subjected to repeated freeze−thaw cycles to obtain purified membrane-derived vesicles (PV), which were fused onto the surface of TNPs using a sonication process.[41]

The resulting PTNPs had an average particle size of 140.3 nm, which was 16 nm larger than the uncoated TNPs, and possessed a surface charge equivalent to that of the PVs, which was measured as −21.9 mV using dynamic light scattering (DLS) (Figure 2b). The increased size compared with TNPs

DOI: 10.1021/acs.nanolett.9b01282
Nano Lett. 2019, 19, 4470−4477

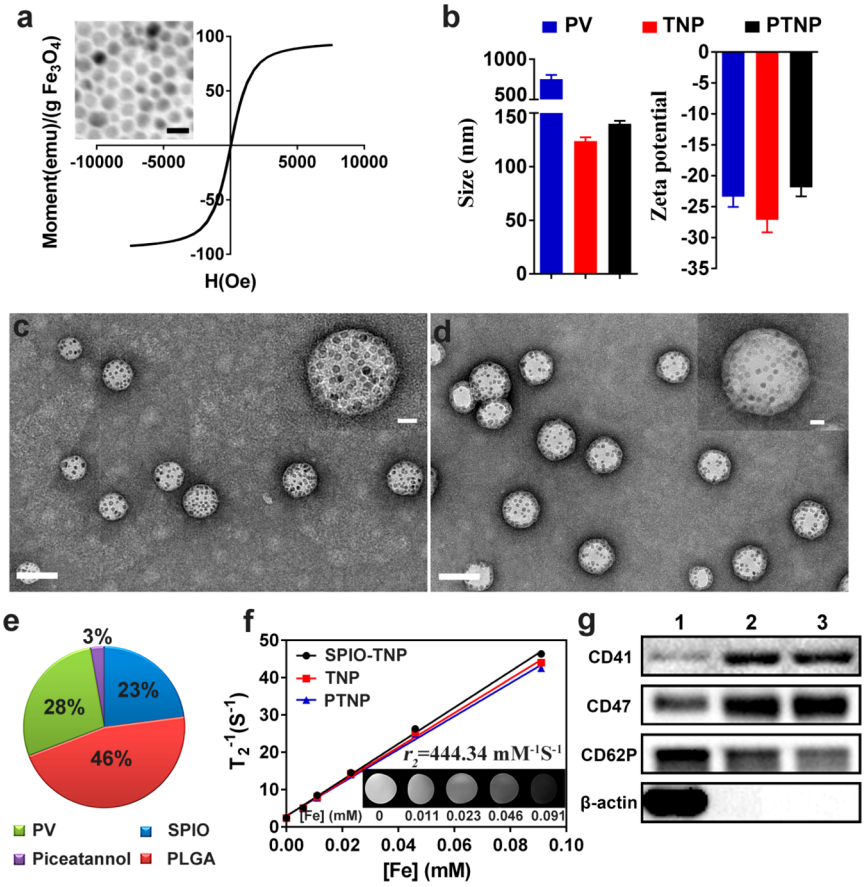

Figure 2. Characterization of PTNPs. (a) Room-temperature hysteresis loop and TEM image of SPIO. (b) Particle sizes and ζ potentials of the platelet vesicles, TNPs, and PTNPs, respectively. Error bars indicate SD (n = 3). Representative TEM images of TNPs (c) and PTNPs (d). Scale bar = 100 nm. The inset shows a single nanoparticle; scale bar = 20 nm. (e) Mass fractions of the different components of PTNPs. (f) T_2 relaxation rate values (R_2) of various nanoparticles at different iron concentrations. The inset shows R_2 values of PTNPs and their T_2-weighted MRI images at different iron concentrations. (g) CD41, CD47, and P-selectin in platelets (1), platelet vesicles (PV) (2), and PTNPs (3) determined by Western blot assay. β-actin was used as a control.

and the similar surface charge to PVs indicated the existence of platelet membranes on the TNPs, and this was further confirmed by transmission electron microscopy (TEM) images demonstrating that PTNPs displayed a unilamellar membrane over their polymeric cores (Figure 2c,d). Moreover, evenly distributed SPIO were observed within both uncoated and coated spherical nanoparticles. We also verified the successful coating by platelet membranes through colocalization of rhodamine-labeled TNPs and DiO-labeled platelet vesicles (Figure S3). In addition, the improved colloidal stability of PTNPs and the slow release of piceatannol from PTNPs in a solution of pH 7.4 phosphate buffered saline (PBS) and fetal bovine serum (FBS) (Figure S4, S5) both suggest a protective effect of platelet membranes during circulation.[42]

To fully understand the exact composition of PTNPs, we quantified the mass fraction of each component including PLGA, SPIO, piceatannol, and the platelet membrane (Figure 2e, Table S1). The drug-loading capability of SPIO and piceatannol were 22.95% and 2.77%, as measured using inductively coupled plasma atomic emission spectrometry (ICP-AES) and high-performance liquid chromatography (HPLC), respectively. The platelet membrane mass, which was obtained using the difference between the weights of PTNPs and TNPs, made up 28.06% of the whole PTNP. It was reported that membrane proteins make up ~40% of the total cell membrane mass.[43] Accordingly, the effective utilization rate of platelet membranes was calculated at approximately 19.5%, based on an optimized weight ratio of membrane proteins to TNPs of approximately 0.8 (w:w) (Figure S6). From a component analysis, we found that SPIO exhibited a relatively high loading efficiency, which may enhance negative contrast in T_2-weighted MRI images.[40] To confirm the MRI contrast-enhancing effect of PTNPs, various nanoparticle dispersions were evaluated using a 7.0 T MRI system. The T_2-weighted relaxation rate value (R_2) of PTNPs was calculated as 444.34 mM^{-1} S^{1-} (Figure 2f), which was close to that of TNPs, suggesting that the platelet membrane coating does not affect MRI functionality, and that PTNPs are suitable as a T_2 contrast agent.

The membrane proteins of PTNPs are strongly linked to their platelet-mimetic functions. To analyze the membrane proteins of PTNPs, protein profiles were determined using Coomassie Blue staining (Figure S7). Platelets and PVs were also prepared in parallel for comparison. There was no significant variation among membrane proteins in these three forms. PTNPs retained most of the platelet membrane proteins in a highly concentrated manner. Among these proteins, some specific protein markers, including CD41, P-selectin, and CD47, were detected on PTNPs using Western blotting (Figure 2g). CD41, also known as integrin αIIbβ3, is a typical platelet-associated protein and plays a crucial role in coagulation.[44] CD47 acts as a "don't eat me" signal to

DOI: 10.1021/acs.nanolett.9b01282
Nano Lett. 2019, 19, 4470−4477

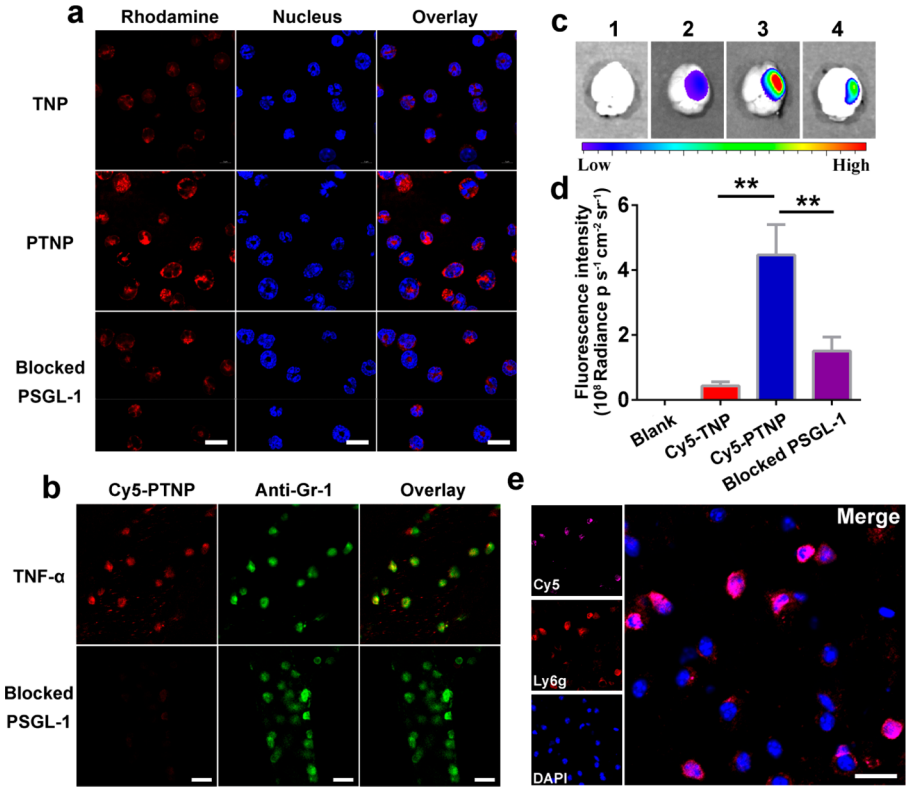

Figure 3. Specific recognition by PTNPs of inflammatory neutrophils *in vitro* and *in vivo*. (a) CLSM images of mouse neutrophils after incubation with rhodamine-labeled PNPs and PTNPs (red). The mouse neutrophils were prestimulated with 10 μM fMLF and stained with DAPI (blue). Neutrophils blocked with an anti-PSGL-1 antibody were used as a control. Scale bar = 10 μm. (b) Intravital images of cremaster muscle venules of mice who had undergone intrascrotal administration of TNF-α (0.5 μg) followed by an intravenous infusion of Cy5-loaded PTNPs (red) and Alex Fluor 488-labeled anti-Gr-1 antibody (green). Mice injected with 50 μg of anti-PSGL-1 antibody were used as a control. Scale bar = 20 μm. (c) *Ex vivo* fluorescence imaging of ischemic brains treated with various Cy5-loaded nanoparticles. (1) Blank; (2) Cy5-TNPs; (3) Cy5-PTNPs; (4) Blocked PSGL-1. (d) Quantification of the fluorescent intensity of ischemic brains. Error bars indicate SD (n = 3). $^{**}P < 0.01$. (e) Immunofluorescent image of ischemic brain sections from a tMCAO mouse treated with Cy5-labeled PTNPs (purple). Neutrophils were stained with Ly6g (red). Scale bar = 20 μm.

macrophages and improves the immune-evading capabilities of the resulting nanocarriers.[45] To verify the antiphagocytic capabilities of PTNPs, intracellular uptake by mouse macrophage RAW264.7 cells was visualized using confocal laser scanning microscopy (CLSM). As expected, PTNPs exhibited the lowest macrophage uptake (Figure S8). It was further confirmed by ICP-AES analysis that the cellular uptake of PTNPs was reduced about 50% compared with TNPs (Figure S9), which is mainly attributed to the fact that CD47 on PTNPs restricted the uptake by macrophage cells. In addition, P-selectin, also known as CD62P, is a cell adhesion molecule on the surface of activated platelets that is reported to participate in the initial recruitment of NEs to the injury site during acute inflammation.[34] The existence of P-selectin on PTNPs may help them to recognize activated NEs.

Collectively, we confirmed the successful fusion of platelet vesicles onto TNPs and provided evidence to support the platelet-mimetic functions of PTNPs by demonstrating the presence of specialized platelet surface proteins, which should allow PTNPs to specifically recognize inflammatory NEs.

The prerequisites for PTNPs to be able to alleviate NEs infiltration are their selective and effective accumulation in adherent NEs. To investigate the specific affinity of PTNPs for inflammatory NEs *in vitro*, the intracellular uptake of PTNPs by mouse NEs was measured. The NEs were isolated from mouse bone marrow as reported in our previous studies, with slight modifications.[46] The purity was quantified to be higher than 95% and morphology represented a condensed poly segmented shape (Figure S10). The obtained NEs were prestimulated with 10 μM *N*-formyl-Met-Leu-Phe (fMLF) to mimic inflammatory NEs.[47] First, a cell viability assay was performed, and the effects of nanoparticles on NEs were negligible (Figure S11), thus demonstrating good biocompatibility of PTNPs. Subsequently, NEs were incubated with various rhodamine-labeled nanoparticles and visualized using CLSM (Figure 3a). Resulting images showed that the PTNP group exhibited stronger red fluorescence compared with the TNP group, demonstrating a biomimetic interaction between PTNPs and NEs. Extensive experimental evidence indicates that platelets assist NEs infiltration into inflamed tissue mainly through the interaction of P-selectin on platelets and PSGL-1 on activated NEs.[34] To confirm this, PSGL-1 proteins on NEs were blocked using a specific anti-PSGL-1 monoclonal antibody. The fluorescent intensity of PTNPs within NEs was markedly decreased, suggesting a crucial role for P-selectin in facilitating internalization of PTNPs. In accordance with CLSM images, Prussian blue staining and quantitative analysis using ICP-AES also showed that the PTNP group had the highest uptake, which was about 3.4-fold higher than that of the TNP group, and 2.3-fold higher than that of the blocked PSGL-1 group (Figure S12). Moreover, prestimulated NEs had significantly enhanced internalization of PTNPs compared

DOI: 10.1021/acs.nanolett.9b01282
Nano Lett. 2019, 19, 4470−4477

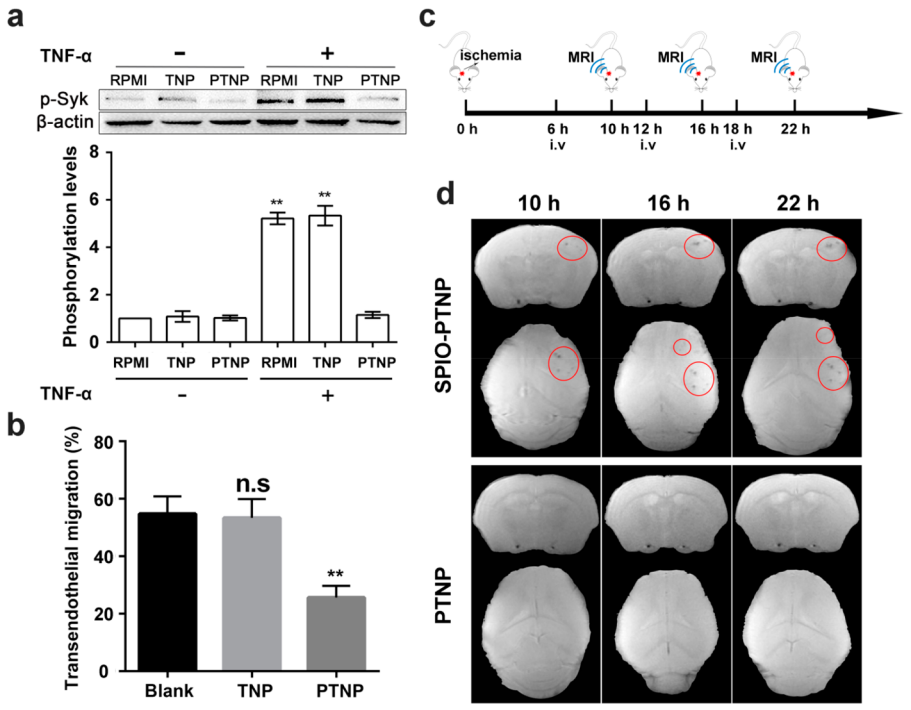

Figure 4. Effective intervention and monitoring by PTNPs on inflammatory neutrophils. (a) Immunoblot image of Syk phosphorylation expression levels in neutrophils treated with TNPs and PTNPs (piceatannol, 200 μM). The culture medium RPMI was used as the negative control. Error bars indicate SD (n = 3). $^{**}P < 0.01$. (b) Percentage of transendothelial neutrophils compared with all neutrophils after intervention with TNPs or PTNPs (piceatannol, 200 μM) on the HUVEC monolayer model. The culture medium RPMI was used as a negative control. Tightly confluent monolayers of HUVECs were stimulated with 10 ng/mL TNF-α for 4 h. Error bars indicate SD (n = 3). $^{**}P < 0.01$. (c) Schematic of the treatment regimen of PTNP administration and the following MRI monitoring in a tMCAO mouse model. (d) T_2*-weighted coronal and transverse images at 10, 16, and 22 h after reperfusion of tMCAO mice that received SPIO-PTNPs and PTNPs 4 h before contrast.

with unstimulated NEs (Figure S13), which further indicates the specific recognition by PTNPs of inflammatory NEs.

Although there is evidence for a high affinity between PTNPs and inflammatory NEs, the *in vivo* recognition ability by PTNPs of inflammatory NEs is inconclusive. To visualize the *in vivo* interactions between nanoparticles and NEs, a scrotal vascular inflammation model was prepared using an intrascrotal injection of TNF-α and was monitored using real-time fluorescence intravital microscopy.[26,48] Postinjection of TNF-α for 3 h, Alexa Fluor 488-labeled antimouse Gr-1 antibody (to label NEs), and Cy5-loaded PTNPs were simultaneously administered intravenously. Using real-time imaging, the PTNPs (red) and adhesive NEs (green) showed marked costaining, and this phenomenon disappeared when anti-PSGL-1 antibody was administered (Figure 3b). These results indicate that PTNPs can target inflammatory NEs through P-selectin on their surface, which should then aid in the sequential internalization of PTNPs. In contrast, injection with saline and TNPs did not exhibit any signs of colocalization with inflammatory NEs. A similar result was found between PTNPs and noninflammatory NEs (Figure S14), which suggests that PTNPs can selectively discern inflammatory NEs from circulating NEs.

We next evaluated the ability of PTNPs to discern inflammatory NEs in the ischemic region. Cy5-labeled PTNPs were intravenously injected into transient middle cerebral artery occlusion (tMCAO) mice 24 h after reperfusion. *Ex vivo* imaging of brains isolated from these mice indicated that PTNPs exhibited higher fluorescent intensity than TNPs in the ischemic region, suggesting a greater accumulation of PTNPs in the ischemic region. In contrast, the fluorescent intensity of PTNPs was markedly decreased following PSGL-1 treatment (Figure 3c). Quantification analysis revealed that the fluorescent intensity in the PTNP group was 10.4-fold higher than in the TNP group, and 3.0-fold higher than in the blocked PSGL-1 group (Figure 3d). This accumulation of PTNPs demonstrates that they retain the intrinsic properties of platelets, in that they can actively search for inflammatory NEs. In addition, immunofluorescent images of brain sections showed that PTNPs and NEs colocalized perfectly in the ischemic region (Figure 3e), while nonimmune isotype antibody IgG exhibited no signal (Figure S15). These results further verify the superior ability of PTNPs to recognize inflammatory NEs in ischemic regions, and their following internalization.

Syk signaling plays a crucial role in the β2-integrin-mediated firm adhesion of inflammatory NEs to vessels. As a selective Syk inhibitor, piceatannol can inhibit Syk phosphorylation (p-Syk) and reverse this pathway.[49,50] To evaluate the inhibitory effect of PTNPs, Western blot assays were used to detect p-Syk expression in NEs and TNF-α-stimulated NEs after incubation with different formulations of piceatannol. TNF-α-stimulated NEs exhibited elevated p-Syk expression (Figure 4a), indicating massive NEs activation. After treatment with PTNPs, p-Syk expression in TNF-α-stimulated NEs was abolished, whereas treatment with TNPs had no visible down-regulatory effect, probably owing to insufficient NEs internalization. Next, NEs adhesion and infiltration with PTNP treatment were assayed on a human umbilical vein endothelial cell (HUVEC) monolayer model.[51] Compared with controls, PTNPs significantly reduced the numbers of adhered and migrated NEs (Figure 4b, Figure S16), which was also verified

DOI: 10.1021/acs.nanolett.9b01282
Nano Lett. 2019, 19, 4470−4477

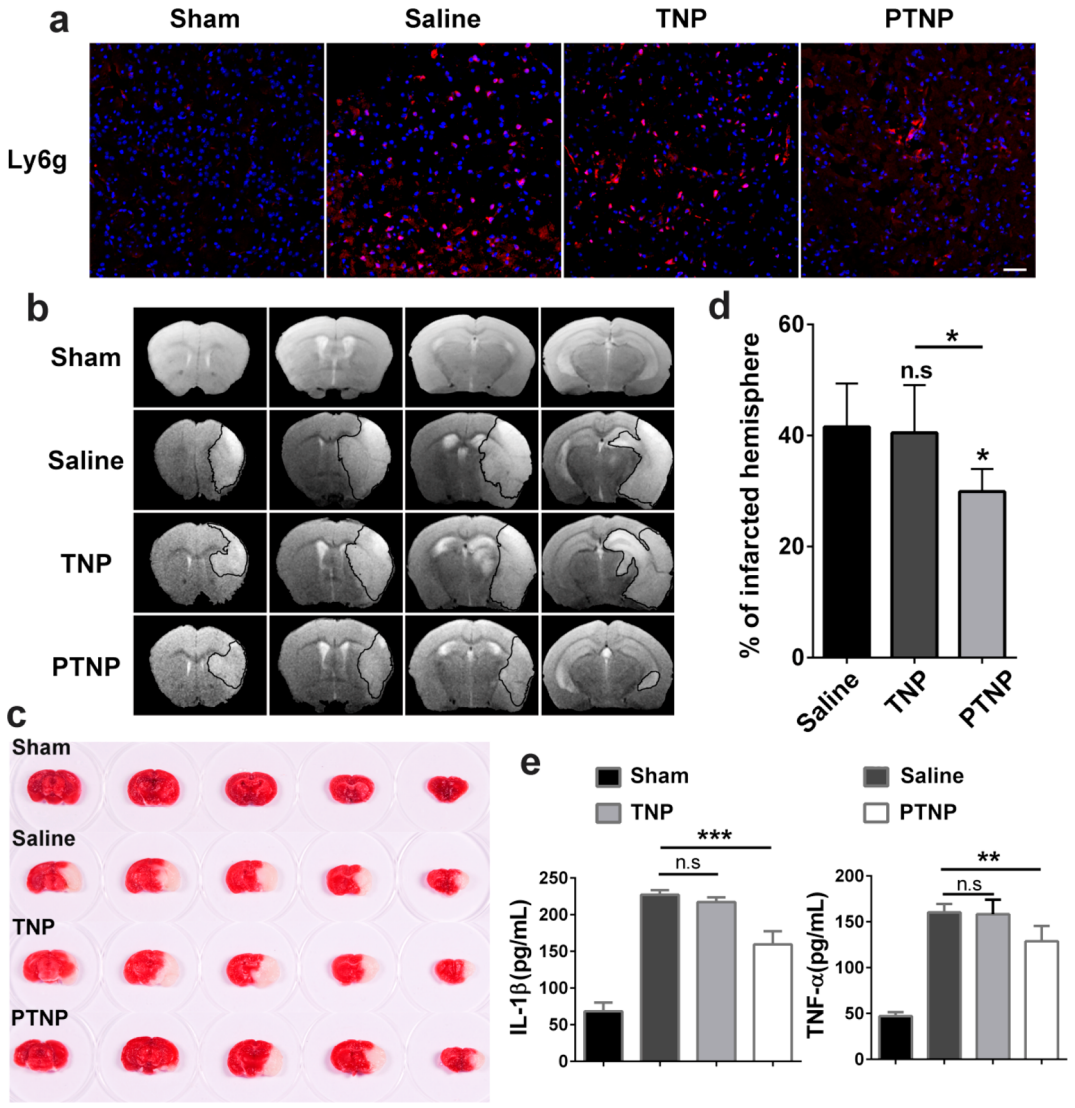

Figure 5. *In vivo* therapeutic efficacy of PTNPs on tMCAO mice. (a) CLSM images of neutrophil infiltration in ischemic brain regions after treatment with saline, TNPs, and PTNPs. Neutrophils were immunostained with anti-Ly6g antibody (red) and nuclei were stained using DAPI (blue). Scale bar: 50 μm. (b) T_2-weighted images of ischemic brains at 24 h in tMCAO mice treated with saline, TNPs, and PTNPs. The black curve indicates the infarct region. (c) 2,3,5-Triphenyltetrazolium chloride (TTC)-stained images of brain slices from the saline-, TNP-, and PTNP-treated tMCAO mice. The white region indicates the infarct region. (d) Quantification of the infarction volumes in saline-, TNP-, and PTNP-treated tMCAO mice. Error bars indicate SD (n = 5). *P < 0.05. (e) Expression levels of IL-1β and TNF-α in the brains of tMCAO mice treated with saline, TNPs, and PTNPs. Error bars indicate SD (n = 5). **P < 0.01, ***P < 0.001.

using a flow cytometry quantification assay (Figure S17). PTNPs can therefore effectively inhibit Syk phosphorylation and impair the outside-in β2 integrin signaling, thereby significantly alleviating NEs adhesion and migration.

To monitor whether PTNPs can ameliorate NEs infiltration in AIS, we constructed a murine tMCAO model for *in vivo* studies. These models were intravenously administered with PTNPs or SPIO-PTNPs (only SPIO-loaded PTNPs) every 6 h followed by MRI detection 4 h later (Figure 4c). Moreover, T_2* weighted sequences of tMCAO mice prior to each administration of SPIO-PTNPs or PTNPs were also acquired to exclude the presence endogenous sources of negative contrast (Figure S18). Mice treated with SPIO-PTNPs exhibited a marked MRI contrast effect, which manifested as intensely low signal areas with a punctate distribution on the ipsilateral side of ischemic brain tissue (Figure 4d). Additionally, the punctate regions of signal loss grew more intense over time. Nonspecific retention was almost absent from the contralateral brain region, consistent with *ex vivo* imaging and Prussian blue staining results. Normal mice that underwent the same injection regime with SPIO-TNPs showed no contrast effect (data not shown). In contrast, following treatment with PTNPs, the punctate signal loss was markedly attenuated, indicating the successful detachment of NEs from the activated vascular endothelial cells and into blood circulation, as a result of the piceatannol action. The quantification analysis was further confirmed the significant marked MRI contrast effect between tMCAO mice respectively received SPIO-PTNPs and PTNPs by calculating the total number of dark voxels in the ischemic region (Figure S19). In brief, NEs infiltration could be monitored using MRI after SPIO-PTNPs injection, suggesting the viability of PTNPs for diagnosing AIS. When coloaded with the therapeutic agent, PTNPs can act in acute ischemic stroke and measure treatment

DOI: 10.1021/acs.nanolett.9b01282
Nano Lett. 2019, 19, 4470−4477

outcome in patients and may thus be an effective tool for treating AIS and evaluating the therapeutic effect of this treatment.

Reduced NEs infiltration is closely associated with therapeutic effects in AIS. In addition to using real-time MRI contrast, immunofluorescence and Prussian blue staining images of brain slices were used to evaluate inflammatory NEs infiltration. The infiltration of NEs labeled with Ly6g in mice treated with PTNPs was significantly reduced compared with the TNP group (Figure 5a). Additionally, the Prussian blue staining image from the SPIO-PTNP group showed that iron was mainly distributed in the luminal surfaces or perivascular spaces of cerebral vessels, which is consistent with a previous report of the distribution of recruited NEs in ischemic regions.[52] In contrast, in the PTNP group there was no iron distribution around vessels in the ischemic brain (Figure S20a). The myeloperoxidase (MPO) activity was also markedly reduced when treating mice with PTNPs (Figure S21). These results provide further evidence that PTNPs can efficiently detach NEs from activated vascular endothelial cells and release them into circulation. However, it was no accident that most of the iron was found in the spleen and liver of the animals in both the TNP and PTNP groups (Figure S20b).

The mice treated with PTNPs also exhibited higher neurological scores and decreased infarct volumes (Figure 5b,c; Figure S22). In addition, quantification analysis showed that the infarct volume of mice treated with PTNPs was significantly decreased, by approximately 26.2% compared with that of mice treated with TNPs (Figure 5d). The levels of inflammatory factors, such as TNF-α and IL-1β, in infarct half-brains were also significantly decreased following PTNPs treatment (Figure 5e), which was beneficial in AIS because of its alleviation of inflammation. As demonstrated by these experiments, intervening in the adhesion and migration of inflammatory NEs is an effective way to treat AIS. The delivery of piceatannol via PTNPs can improve its therapeutic effect via the selective targeting of inflammatory NEs.

In conclusion, we have developed an NE intervention tactic that involves the use of PTNPs for the effective treatment of AIS and the real-time therapeutic evaluation of this treatment. These biomimetic nanoparticles can effectively recognize inflammatory NEs in cerebral ischemic regions, be internalized by taking advantage of the specific affinity between platelets and polarized NEs, and release the NEs intervention drug, thus leading to an effective reduction of infiltrating NEs in cerebral ischemic regions. Importantly, we were able to monitor the infiltrating NEs associated with the therapeutic effect using the same biomimetic nanoparticles. This strategy can reduce infarct size and improve neurological outcomes, and it exhibits a very good effect on AIS and the real-time evaluation of its own efficacy. Its use will provide new insights into the treatment and diagnosis of AIS, and it offers broad potential applications for other inflammatory disorders.

■ ASSOCIATED CONTENT

Supporting Information

The Supporting Information is available free of charge on the ACS Publications website at DOI: 10.1021/acs.nanolett.9b01282.

Expanded materials and methods, Figures S1−S22 of XRD and FT-IR spectra, size distribution histograms, CLSM images, stability and release graphs, quantification of total membrane proteins on PTNP, SDS-PAGE analysis, uptake images, quantitative analysis of the macrophage uptake, flow cytometric analysis, neutrophil viability after incubation, cellular uptake of TNPs, PTNPs, and Rhodamine labeled PTNP in mouse neutrophils, intravital microscopy of neutrophils, specificity of anti-Ly6g antibody in mouse neutrophils, evaluation of neutrophil adhesion to a HUVEC monolayer, FACS analysis ,T2*-weighted coronal and transverse images, total number of dark voxels in the ischemic region, brain sample stains, MPO activity, effects of TNPs and PTNPs on neurological scores, and Table S1 of content data (PDF)

■ AUTHOR INFORMATION

Corresponding Authors

*E-mail: zhangcan@cpu.edu.cn. Phone/Fax number: 86-25-83271171.

*E-mail: jucaoyun@cpu.edu.cn. Phone number: 86-25-83271076.

ORCID

Can Zhang: 0000-0003-3529-5438

Author Contributions

C.T., C.W., and C.Z. conceived and designed the research. C.T., C.W., Y.Z., and Y.L. performed the experiments. C.T., C.J., C.W., and L.X. analyzed the data and wrote the manuscript. C.Z. supervised the project. All authors discussed the results and commented on the manuscript.

Notes

The authors declare no competing financial interest.

■ ACKNOWLEDGMENTS

This work was supported by the National Natural Science Foundation of China (81773664, 81473153, 81503003), National Basic Research Program of China (2015CB755504), 111 Project from the Ministry of Education of China and the State Administration of Foreign Expert Affairs of China (No. 111-2-07, B17047), Fundamental Research Funds for the Central Universities of China (2632017ZD06), the Open Project of State Key Laboratory of Natural Medicines (No. SKLNMZZCX201811), and "Double First-Class" University project (CPU2018GY47, CPU2018GF10). The authors thank the public platform of State Key Laboratory of Natural Medicines for assistance with Confocal Microscopy and Flow Cytometry.

■ REFERENCES

(1) GBD 2016 DALYs and HALE.. *Lancet* **2017**, *390* (10100), 1260−1344.

(2) Brott, T.; Bogousslavsky, J. *N. Engl. J. Med.* **2000**, *343* (10), 710−722.

(3) Krishnamurthi, R. V.; Feigin, V. L.; Forouzanfar, M. H.; Mensah, G. A.; Connor, M.; Bennett, D. A.; Moran, A. E.; Sacco, R. L.; Anderson, L. M.; Truelsen, T.; O'Donnell, M.; Venketasubramanian, N.; Barker-Collo, S.; Lawes, C. M. M.; Wang, W. Z.; Shinohara, Y.; Witt, E.; Ezzati, M.; Naghavi, M.; Murray, C.; Dis, G. B.; R. F. S. G; Grp, G. S. E. *Lancet Glob Health* **2013**, *1* (5), E259−E281.

(4) Hacke, W.; Kaste, M.; Bluhmki, E.; Brozman, M.; Davalos, A.; Guidetti, D.; Larrue, V.; Lees, K. R.; Medeghri, Z.; Machnig, T.; Schneider, D.; von Kummer, R.; Wahlgren, N.; Toni, D.; Investigators, E. *N. Engl. J. Med.* **2008**, *359* (13), 1317−1329.

(5) Saver, J. L.; Levine, S. R. *Lancet* **2010**, *375* (9727), 1667−1668.

DOI: 10.1021/acs.nanolett.9b01282
Nano Lett. 2019, 19, 4470−4477

(6) Bluhmki, E.; Chamorro, A.; Davalos, A.; Machnig, T.; Sauce, C.; Wahlgren, N.; Wardlaw, J.; Hacke, W. *Lancet Neurol.* **2009**, *8* (12), 1095−1102.
(7) Hacke, W.; Donnan, G.; Fieschi, C.; Kaste, M.; von Kummer, R.; Broderick, J. P.; Brott, T.; Frankel, M.; Grotta, J. C.; Haley, E. C.; Kwiatkowski, T.; Levine, S. R.; Lewandowski, C.; Lu, M.; Lyden, P.; Marler, J. R.; Patel, S.; Tilley, B. C.; Albers, G.; Brott, T.; Grotta, J.; Bluhmki, P. E.; Wilhelm, M.; Hamilton, S.; Investigators, A. S. G.; Investigators, E. S. G.; Investigato, N. R.-P. S. G. *Lancet* **2004**, *363* (9411), 768−774.
(8) Moskowitz, M. A.; Lo, E. H.; Iadecola, C. *Neuron* **2010**, *67* (2), 181−198.
(9) Chamorro, A.; Dirnagl, U.; Urra, X.; Planas, A. M. *Lancet Neurol.* **2016**, *15* (8), 869−881.
(10) George, P. M.; Steinberg, G. K. *Neuron* **2015**, *87* (2), 297−309.
(11) Ross, A. M.; Hurn, P.; Perrin, N.; Wood, L.; Carlini, W.; Potempa, K. *J. Stroke Cerebrovasc Dis* **2007**, *16* (5), 203−207.
(12) Jin, R.; Yang, G.; Li, G. *J. Leukocyte Biol.* **2010**, *87* (5), 779−789.
(13) Shichita, T.; Sakaguchi, R.; Suzuki, M.; Yoshimura, A. *Front. Immunol.* **2012**, *3*, 132.
(14) Buck, B. H.; Liebeskind, D. S.; Saver, J. L.; Bang, O. Y.; Yun, S. W.; Starkman, S.; Ali, L. K.; Kim, D.; Villablanca, J. P.; Salamon, N.; Razinia, T.; Ovbiagele, B. *Stroke* **2008**, *39* (2), 355−360.
(15) Kumar, A. D.; Boehme, A. K.; Siegler, J. E.; Gillette, M.; Albright, K. C.; Martin-Schild, S. *J. Stroke Cerebrovasc Dis* **2013**, *22* (7), e111−117.
(16) Lakhan, S. E.; Kirchgessner, A.; Hofer, M. *J. Transl. Med.* **2009**, DOI: 10.1186/1479-5876-7-97.
(17) Zhang, K.; Tu, M.; Gao, W.; Cai, X.; Song, F.; Chen, Z.; Zhang, Q.; Wang, J.; Jin, C.; Shi, J.; Yang, X.; Zhu, Y.; Gu, W.; Hu, B.; Zheng, Y.; Zhang, H.; Tian, M. *Nano Lett.* **2019**, *19* (5), 2812−2823.
(18) Jickling, G. C.; Liu, D.; Ander, B. P.; Stamova, B.; Zhan, X.; Sharp, F. R. *J. Cereb. Blood Flow Metab.* **2015**, *35* (6), 888−901.
(19) Schofield, Z. V.; Woodruff, T. M.; Halai, R.; Wu, M. C. L.; Cooper, M. A. *Shock* **2013**, *40* (6), 463−470.
(20) Soriano, S. G.; Coxon, A.; Wang, Y. F.; Frosch, M. P.; Lipton, S. A.; Hickey, P. R.; Mayadas, T. N. *Stroke* **1999**, *30* (1), 134−139.
(21) Zhang, L.; Zhang, Z. G.; Zhang, R. L.; Lu, M.; Krams, M.; Chopp, M. *Stroke* **2003**, *34* (7), 1790−1795.
(22) Zhang, Z. G.; Chopp, M.; Tang, W. X.; Jiang, N.; Zhang, R. L. *Brain Res.* **1995**, *698* (1−2), 79−85.
(23) Chopp, M.; Zhang, R. L.; Chen, H.; Li, Y.; Jiang, N.; Rusche, J. R. *Stroke* **1994**, *25* (4), 869−875.
(24) Chen, H.; Chopp, M.; Zhang, R. L.; Bodzin, G.; Chen, Q.; Rusche, J. R.; Todd, R. F. *Ann. Neurol.* **1994**, *35* (4), 458−463.
(25) Yenari, M. A.; Kunis, D.; Sun, G. H.; Onley, D.; Watson, L.; Turner, S.; Whitaker, S.; Steinberg, G. K. *Exp. Neurol.* **1998**, *153* (2), 223−233.
(26) Wang, Z. J.; Li, J.; Cho, J.; Malik, A. B. *Nat. Nanotechnol.* **2014**, *9* (3), 204−210.
(27) Veiseh, O.; Gunn, J. W.; Zhang, M. Q. *Adv. Drug Delivery Rev.* **2010**, *62* (3), 284−304.
(28) Yoo, J. W.; Irvine, D. J.; Discher, D. E.; Mitragotri, S. *Nat. Rev. Drug Discovery* **2011**, *10* (7), 521−535.
(29) Zhang, C.; Ling, C. L.; Pang, L.; Wang, Q.; Liu, J. X.; Wang, B. S.; Liang, J. M.; Guo, Y. Z.; Qin, J.; Wang, J. X. *Theranostics* **2017**, *7* (13), 3260−3275.
(30) Chu, D. F.; Dong, X. Y.; Zhao, Q.; Gu, J. K.; Wang, Z. J. *Adv. Mater.* **2017**, *29* (27), 1701021.
(31) Miettinen, H. M.; Gripentrog, J. M.; Lord, C. I.; Nagy, J. O. *PLoS One* **2018**, *13* (7), e0200444.
(32) Soehnlein, O. *Eur. J. Clin. Invest.* **2018**, *48* (2), e12871.
(33) Lisman, T. *Cell Tissue Res.* **2018**, *371* (3), 567−576.
(34) Sreeramkumar, V.; Adrover, J. M.; Ballesteros, I.; Cuartero, M. I.; Rossaint, J.; Bilbao, I.; Nacher, M.; Pitaval, C.; Radovanovic, I.; Fukui, Y.; McEver, R. P.; Filippi, M. D.; Lizasoain, I.; Ruiz-Cabello, J.; Zarbock, A.; Moro, M. A.; Hidalgo, A. *Science* **2014**, *346* (6214), 1234−1238.
(35) Lu, Y.; Xu, Y. J.; Zhang, G. B.; Ling, D. S.; Wang, M. Q.; Zhou, Y.; Wu, Y. D.; Wu, T.; Hackett, M. J.; Kim, B. H.; Chang, H.; Kim, J.; Hu, X. T.; Dong, L.; Lee, N.; Li, F. Y.; He, J. C.; Zhang, L.; Wen, H. Q.; Yang, B.; Choi, S. H.; Hyeon, T.; Zou, D. H. *Nature Biomedical Engineering* **2017**, *1* (8), 637−643.
(36) Zhao, Y.; Peng, J.; Li, J.; Huang, L.; Yang, J.; Huang, K.; Li, H.; Jiang, N.; Zheng, S.; Zhang, X.; Niu, Y.; Han, G. *Nano Lett.* **2017**, *17* (7), 4096−4100.
(37) Hu, Q.; Qian, C.; Sun, W.; Wang, J.; Chen, Z.; Bomba, H. N.; Xin, H.; Shen, Q.; Gu, Z. *Adv. Mater.* **2016**, *28* (43), 9573−9580.
(38) Chen, Z.; Hu, Q.; Gu, Z. *Acc. Chem. Res.* **2018**, *51* (3), 668−677.
(39) Xu, Z. C.; Shen, C. M.; Hou, Y. L.; Gao, H. J.; Sun, S. S. *Chem. Mater.* **2009**, *21* (9), 1778−1780.
(40) Kim, J.; Lee, J. E.; Lee, S. H.; Yu, J. H.; Lee, J. H.; Park, T. G.; Hyeon, T. *Adv. Mater.* **2008**, *20* (3), 478−483.
(41) Hu, C. M.; Fang, R. H.; Wang, K. C.; Luk, B. T.; Thamphiwatana, S.; Dehaini, D.; Nguyen, P.; Angsantikul, P.; Wen, C. H.; Kroll, A. V.; Carpenter, C.; Ramesh, M.; Qu, V.; Patel, S. H.; Zhu, J.; Shi, W.; Hofman, F. M.; Chen, T. C.; Gao, W.; Zhang, K.; Chien, S.; Zhang, L. *Nature* **2015**, *526* (7571), 118−121.
(42) Hu, Q.; Sun, W.; Qian, C.; Wang, C.; Bomba, H. N.; Gu, Z. *Adv. Mater.* **2015**, *27* (44), 7043−7050.
(43) Gao, J.; Chu, D.; Wang, Z. *J. Controlled Release* **2016**, *224*, 208−216.
(44) Bennett, J. S. *Ann. N. Y. Acad. Sci.* **2001**, *936*, 340−354.
(45) Grimsley, C.; Ravichandran, K. S. *Trends Cell Biol.* **2003**, *13* (12), 648−656.
(46) Xue, J. W.; Zhao, Z. K.; Zhang, L.; Xue, L. J.; Shen, S. Y.; Wen, Y. J.; Wei, Z. Y.; Wang, L.; Kong, L. Y.; Sun, H. B.; Ping, Q. N.; Mo, R.; Zhang, C. *Nat. Nanotechnol.* **2017**, *12* (7), 692−700.
(47) Hahm, E.; Li, J.; Kim, K.; Huh, S.; Rogelj, S.; Cho, J. *Blood* **2013**, *121* (19), 3789−3800.
(48) Kim, K. H.; Barazia, A.; Cho, J. *J. Visualized Exp.* **2013**, *74*, e50329.
(49) Zarbock, A.; Lowell, C. A.; Ley, K. *Immunity* **2007**, *26* (6), 773−783.
(50) Geahlen, R. L.; McLaughlin, J. L. *Biochem. Biophys. Res. Commun.* **1989**, *165* (1), 241−245.
(51) Finisguerra, V.; Di Conza, G.; Di Matteo, M.; Serneels, J.; Costa, S.; Thompson, A. A. R.; Wauters, E.; Walmsley, S.; Prenen, H.; Granot, Z.; Casazza, A.; Mazzone, M. *Nature* **2015**, *522* (7556), 349.
(52) Farr, T. D.; Lai, C. H.; Grunstein, D.; Orts-Gil, G.; Wang, C. C.; Boehm-Sturm, P.; Seeberger, P. H.; Harms, C. *Nano Lett.* **2014**, *14* (4), 2130−2134.

DOI: 10.1021/acs.nanolett.9b01282
Nano Lett. 2019, 19, 4470−4477